Nozzle Geometry Effects on Supersonic Jet Interaction

R. W. Wlezien*
McDonnell Douglas Research Laboratories, St. Louis, Missouri

The coupled interaction of jets from two nominally identical convergent/divergent nozzles is examined as a function of nozzle spacing. The screech modes of two coupled jets correspond to those observed from single plumes, but the modal amplitudes are strongly dependent on nozzle spacing. For closely spaced nozzles, coupling occurs at low jet Mach numbers and is suppressed at high Mach numbers. The converse is true for large spacing. The amplitude of the coupled jets is independent of the nozzle design Mach number, unlike the screech amplitudes of isolated plumes that decrease near the design point. Interference between the plumes and the relative phasing of the acoustic sources are proposed as mechanisms for the geometry dependence of the jet coupling.

Introduction

THE generation of high-intensity narrow-band noise, commonly referred to as screech, has been studied in isolated supersonic jets over the past 30 years (see, for example, the review article by Seiner[1]). The propulsion systems of many high-performance aircraft use twin-nozzle configurations; thus, interest has been growing in the instability of multiple interacting supersonic plumes.

Clauss, Wright, and Bowie[2] investigated several full-scale multiple-jet configurations and observed highly directive noise reduction, which they attributed to acoustic shielding. More recently, damage has been observed on external nozzle flaps of aircraft with closely spaced twin nozzles. Berndt[3] conducted wind-tunnel tests of modified B-1A nozzles and aft fairings and found that the pattern of greatest dynamic pressures on the exterior of the nozzles match the damage pattern observed in the flight-test program.

In two recent papers, Seiner, Manning, and Ponton[4,5] defined the mechanism of twin-plume resonance and showed that interacting plumes generate dynamic pressures exceeding the fatigue failure limit for metallic aircraft structures. In Ref. 4, the plume resonance phenomenon was shown to be related to the screech instability observed in single jets. However, test were limited to choked-tube nozzles. In Ref. 5, more realistic convergent/divergent (C/D) nozzles were investigated at both model and full scale. For the 4.7% model, plume coupling caused increased dynamic pressures for the B-mode helical instability. Full-scale static tests produced frequencies predicted on the basis of model-scale data, although the amplitudes were lower than those measured in the laboratory.

The purpose of this paper is to clarify the role of jet spacing in dynamic plume interaction. In previous studies, the nozzle spacing was based on configurations of aircraft that experienced fatigue failures in flight. A parametric investigation of twin-plume interaction as a function of nozzle spacing is presented here to characterize the regimes of high dynamic pressure. Detailed flow visualization and laser velocimetry are used to provide further insight into the mechanisms of screech; this insight is required to implement noise-control strategies for current and future aircraft designs.

Experimental Approach

A model-scale investigation of plume interaction was conducted in the McDonnell Douglas Research Laboratories Aerodynamic Noise Facility. In this facility, dry compressed air is supplied from storage bottles and is controlled by a series of 14 valves with choked orifices having cross-sectional areas in a binary sequence. Plenum pressure is maintained within 0.2% of the specified value. The airstream is silenced by a series of high-capacity mufflers and is efficiently turned through corners containing turning vanes. A low-turbulence-level flow is produced by a 300-mm-diam settling chamber containing honeycomb and screens.

A contraction with an 11.5:1 area ratio and hyperelliptic cross sections were used as a transition from the circular cross section to a 63.5-mm × 127-mm rectangle. A dual-contraction section followed with side-by-side square inlets and 38-mm-diam circular exits. The nozzles were connected to the contractions by 200-mm lengths of flexible tubing that permitted variable spacing between the nozzles. A typical nozzle configuration is shown in Fig. 1.

The nozzle sections had convergent/divergent profiles with nominal throat diameters $d_t = 25.4$ mm, exit diameters $d = 27.3$ mm, and an area ratio of 1.15. The design Mach number for these nozzles was 1.48. Because of manufacturing tolerances, the two nozzles were not exactly identical, with nozzle 2 having a smoother internal contour.

The normalized center-to-center spacing s/d of the nozzles was carried over the range $1.8 \geq s/d \geq 3.2$. A single 3.2-mm B&K microphone was positioned midway between the nozzles in the nozzle exit plane. The spectrum of the microphone signal was computed by an HP 3582A spectrum analyzer under control of the VAXlab laboratory microcomputer system. Ensemble-averaged spectra were transferred to the microcomputer for further analysis and plotting. Overall sound pressure levels were determined by use of piston-phone calibrations.

Phase-conditioned schlieren and shadowgraph video images were obtained with the conditioning scheme described in Ref. 6. The video frames were digitized on a Gould 8500 image-

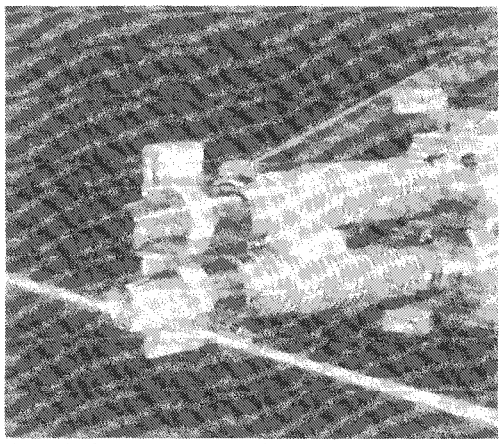

Fig. 1 A typical twin-nozzle configuration; two-component laser velocimeter with sensing volume positioned near exit of lower nozzle.

Presented as Paper 87-2694 at the AIAA 11th Aeroacoustics Conference; received Dec. 28, 1987; revision received Oct. 27, 1988.

*Scientist. Senior Member AIAA.

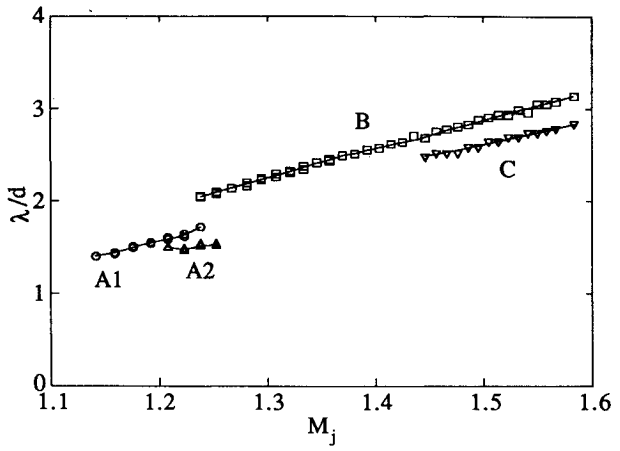

Fig. 2 Single-nozzle screech modes; composite plot for nozzles 1 and 2.

processing system and were dispalyed on a Silicon Graphics IRIS 2400T work station. The enhancement software removed background intensity radient by bilinear interpolation of the intensity at the four corners of the image and achieved enhanced contrast by linear expansion of the gray-level histogram.

Two-component velocity measurements were obtained with a DANTEC laser Doppler velocimeter (LDV) system. The flow was seeded with a polyethylene glycol mist of 1-μm-diam particles through a port upstream of the mufflers in the flow system. A secondary seeder was used to maintain nearly identical particle density in the room air. The LDV signals were acquired and processed on the VAXlab system through a high-speed DMA interface. The interface permitted sustained data acquisition rates of over 10 kilobursts/s.

A grid of 33 transverse by 35 streamwise points were generated to cover the range $-0.85 \le y/d \le 0.85$ and $0.1 \le x/d \le 4.0$. The grid points were uniformly distributed in the axial direction and clustered in the jet shear layers to provide greatest spatial resolution in the regions having large velocity gradients. Detailed measurements were restricted to a single jet, although baseline measurements of the twin plumes verified the symmetry of the jet system. A total of 8000 bursts were acquired at each grid point with 5/8-cycle counting and coincidence detection used to qualify each burst.

Temporal data were provided by a time-between-bursts counter with a 1-μs clock. A screech synchronization pulse was derived from the bandpass-filtered microphone signal thus allowing determination of the relative phase at which each burst was acquired.

Results

Acoustic Measurements

Acoustic spectra were obtained for 30 nozzle pressure ratios between 2.0 and 4.0 for individual nozzles and for the dual-nozzle configuration at eight different spacings: $s/d = 1.8$, 2.0, 2.2, 2.4, 2.6, 2.8, 3.0, and 3.2. This data set included 300 spectra, each with 250 discrete frequencies from 0 to 10 kHz.

An automated processing algorithm was developed to track the magnitude and frequency of the screech peaks. Only those peaks with an amplitude greater than 120 dB were considered. The normalized wavelength λ/d corresponding to the peaks was cast as a function of M_j, the Mach number of a perfectly expanded jet at a given pressure ratio. Other investigators have shown that the dependence of λ/d on M_j is generally linear. Linear trends in the data were detected and low-amplitude peaks deviating from the trends were eliminated.

Figure 2 shows the single-nozzle screech modes as a function of M_j. Each jet develops axisymmetric A1 and A2 modes at low M_j and helical B and C modes at higher M_j. The mode-switching phenomenon has been well documented in isolated round jets,[7-9] and the mode notation adopted in literature will be used here. No consistent explanation of mode switching exists at this time, but the phenomena is probably related to changes in shock cell spacing and shear-layer instability growth rates. The modal wavelengths of the two plumes are virtually identical, suggesting similar shock structures in both plumes.

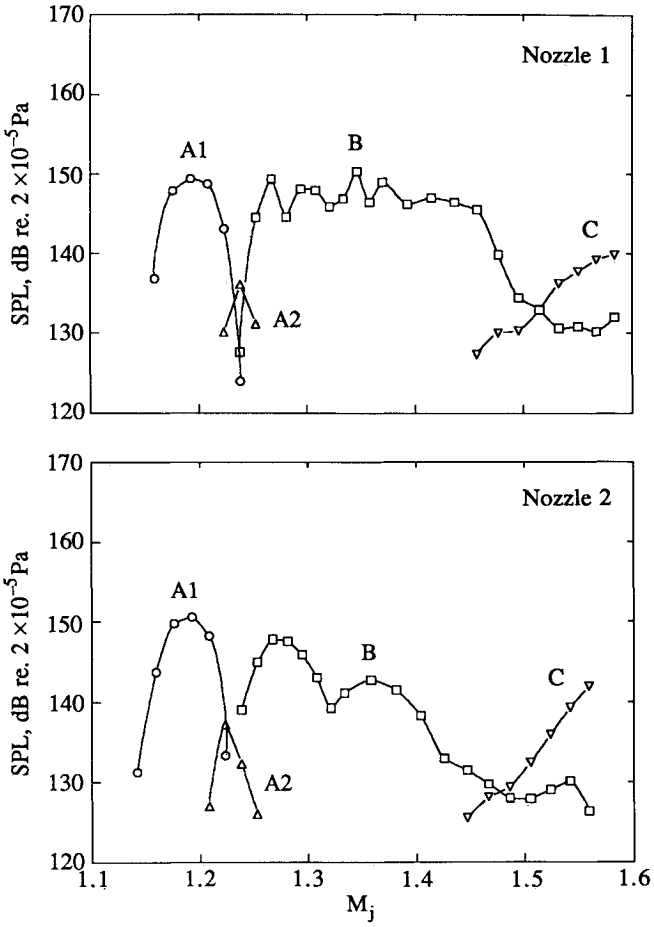

Fig. 3 Single-nozzle screech amplitudes.

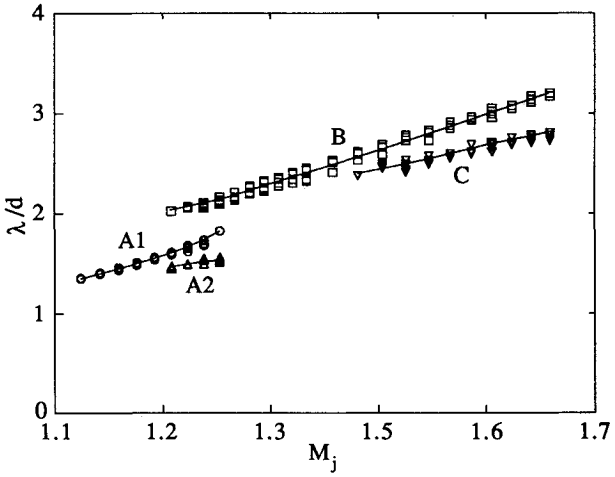

Fig. 4 Composite plot of twin-nozzle screech modes for $1.8 \le s/d \le 3.2$.

The modal amplitudes for the isolated jets are shown in Fig. 3. The microphone used for these measurements was placed 1.6 d from the nozzle centerline, or in the same relative position as for the dual nozzles with $s/d = 3.2$. The A1, A2, and C modes have similar peak amplitudes and dependence on M_j.

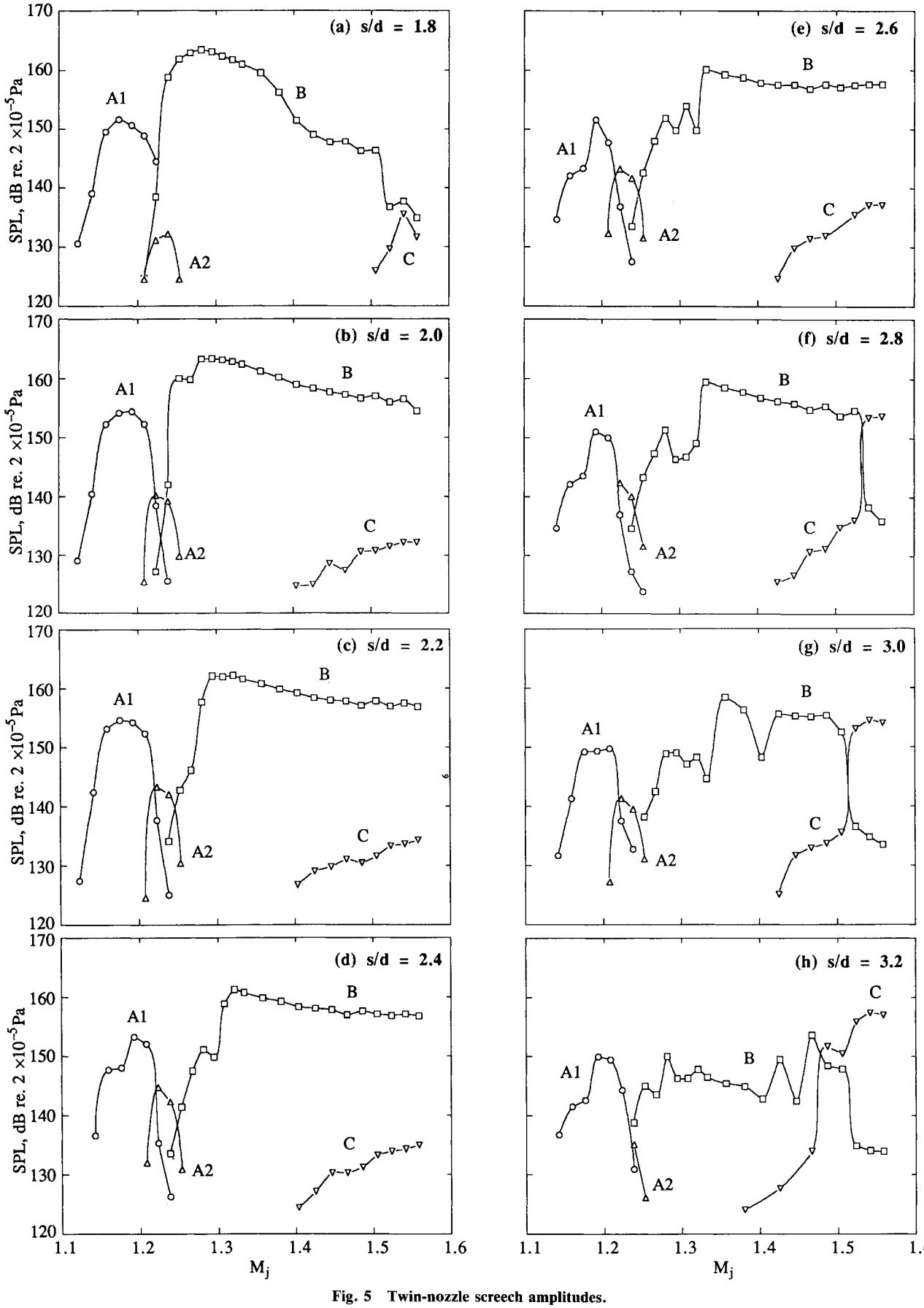

Fig. 5 Twin-nozzle screech amplitudes.

The B mode is apparently more sensitive to nozzle contour, with differences in amplitude as great as 15 dB over the range $1.3 \leq M_j \leq 1.5$. Slight differences into the internal contour of nominally identical nozzles can produce differences in the plumes, as noted in Ref. 5. A local minimum of the acoustic amplitude for each nozzle occurs near $M_j = 1.48$, the design

Mach number and a condition for which the shocks should be weakest. Beyond the design Mach number the plume is underexpanded and the C mode is dominant.

Figure 4 is a composite plot of modal wavelength as a function of Mach number for the eight dual-nozzle spacings studied. The instability modes for the paired nozzles are essentially the same as those observed for the isolated plumes, with no decrease in the identifiable modes as noted in Ref. 5.

Figure 5 summarizes the modal amplitudes as a function of nozzle spacing. Figure 5a shows the characteristic amplitudes for the minimum nozzle spacing, $s/d = 1.8$. For toroidal A1 mode, interaction between the plumes produces no net increase in dynamic pressure; the magnitude is approximately the sum of that from the two isolated jets. However, the B mode is significantly enhanced, particularly for $M_j < 1.4$, and the dynamic pressure is as much as 10 dB greater than the sum of that from the two isolated nozzles. For $M_j > 1.4$, the B mode is enhanced relative to the isolated jets, and the C mode is suppressed. Over the M_j range investigated the C mode is never dominant, and the overall sound pressure level is less than the sum of the isolated jets for $M_j > 1.52$.

A slight increase in nozzle spacing to $s/d = 2.0$ (Fig. 5b) produces a large increase in the B-mode amplitude at high M_j. Plume interaction produces a noise increment of at least 10 dB for all M_j above B-mode onset. As before, the C-mode interaction is strongly suppressed.

A comparison with the data taken through $s/d = 2.6$ (Fig. 5c–e) shows several consistent trends with increased nozzle spacing. The B mode remains dominant for M_j greater than that of the onset of the B mode, with strong plume interaction for large M_j. C-mode amplitudes are suppressed relative to the isolated jets, and the feedback mechanism appears to be modified because of the proximity of the jets. The peak B-mode amplitude shifts to increasing M_j with increasing s/d, with little or no amplitude increment due to plume interaction at lower M_j. Similarly, the A1 mode interaction is strongest for small s/d, with a net increase in amplitude due to plume coupling for $s/d = 2.0$ and 2.2.

The B-mode trends continue thorugh the larger values of s/d (Fig. 5f–h). For $s/d = 3.2$, plume interaction does not occur below $M_j = 1.4$, and the screech amplitudes are suppressed relative to the isolated jets. A dramatic change occurs in the C mode, with strong interaction existing for $s/d = 2.8$ and higher. For $s/d = 3.2$ and M_j approximately 1.5, the screech amplitude increment due to plume interaction is approximately 20 dB.

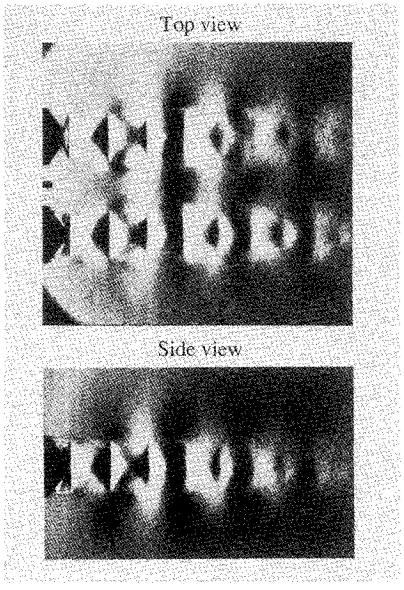

Fig. 6 Schlieren visualization of coupled A1 mode; $s/d = 1.8$, $M_j = 1.19$.

The plume interaction continues to support screech at the nozzle design Mach number. Only at $s/d = 1.8$ is there a decrease in amplitude near the design Mach number of 1.48. There is no similar decrease for any other nozzle spacing. Although the plume should be nominally shock-free near the design point, screech is supported for the twin-nozzle configuration. It is possible that the plumes are ideally expanded in a mean sense at the design point, but oscillate between under- and overexpansion when experiencing screech.

Flow Visualization

Phase-conditioned schlieren and shadowgraph images were obtained for a wide range of flow conditions. The interactions between the plumes can be classified into the following categories: symmetric A1, symmetric B, symmetric C, antisymmetric B, and decoupled. In many instances the modes are inter-

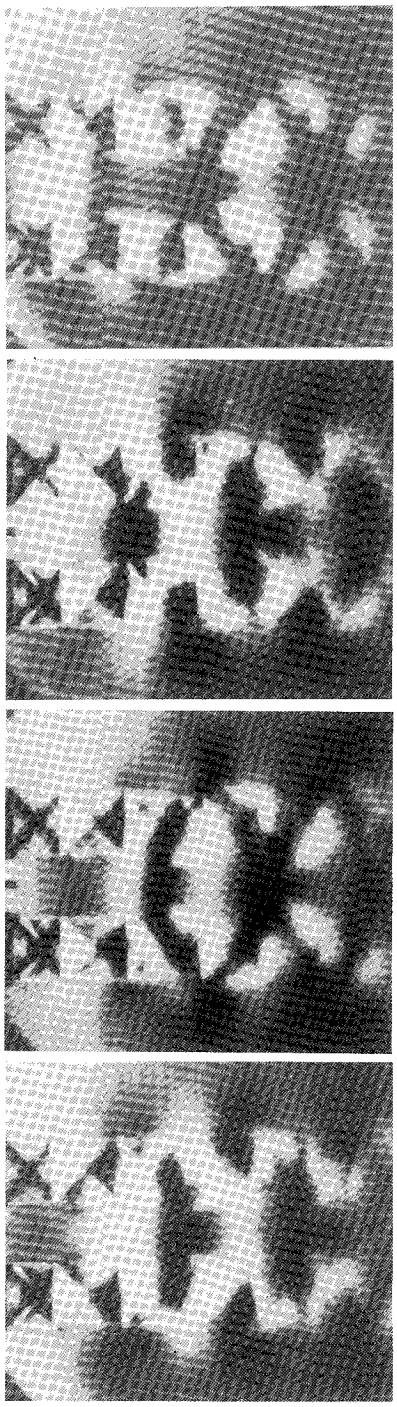

Fig. 7 Schlieren visualization of coupled B mode; $s/d = 1.8$, $M_j = 1.31$.

mittent, with the jets rapidly switching between modes. Ony representative examples are included here.

Figure 6 is schlieren photograph of strong A1 intraction for $s/d = 1.8$ at $M_j = 1.19$. The top and side views are at the same relative phase Ψ. The acoustic perturbations outside the jet are correspondingly axisymmetric. Disturbances in the shear layer are convected downstream from the nozzle lip, and no flapping of the jet core is observed. Shadowgraphs of these jets suggest that the shear-layer disturbances are vortex rings.

Strong B-mode coupling is illustrated in Fig. 7 for $M_j = 1.31$. There is evidence of a helical mode similar to that observed in the isolated plumes, with the helices synchronized in a symmetric, oppositely rotating sense. In Fig. 7a, the third shock cell is displaced outward from the plane of symmetry between the plumes, and the second and fourth cell are diplaced inward. Progressing thorugh 180 deg in phase as shown in Figs. 7b and 7c, the shock cells are observed to pass through the jet axes to a configuration with cells two and four displaced outward and cell three displaced inward. A comparison between the top view (Fig. 7) and the side view (Fig. 8) indicates that the acoustic field is helical, with the upper jet in Fig. 7 oriented as a clockwise helix with respect to the jet axis. The side view also suggests that the plume motion is primarily lateral flapping, similar to the dominant flapping mode of isolated plumes described in Ref. 10. When two plumes are in close proximity, the preferred direction is determined by the mutual influence of the plumes. The flapping is not totally planar, with a slight out-of-plane asymmetry suggested in Fig. 8.

The acoustic perturbation is greatest between the plumes and originates from the vicinity of the third shock cell (Fig. 7a). As phase advances, the disturbance propagates downstream and upstream. This case represents maximal plume interaction, with the greatest dynamic pressures in the internozzle region.

The role of the shear-layer disturbances is further illuminated by the shadowgraph pictures in Fig. 9 for three phases of the screech cycle. These pictures are digitized from continuous video sequences, and the exact phase of each image is not known. In this case $s/d = 1.7$ and $M_j = 1.31$, but the apparent shock spacing is shortened relative to the nozzle spacing because of the characteristics of the video imaging system. At the first phase (Fig. 9a), a disturbance appears in the shear layer between the plumes upstream of the second shock cell. In Fig. 9b the disturbance has been convected past the second cell, and in Fig. 9c it is interacting with the third cell.

When the schlieren visualization is viewed as a continuous sequence, the disturbance appears to be vortical. On the basis of the visualization, the disturbance is strongest between the nozzles. The laser velocimeter measurements discussed in the next section show that the disturbance is present 180 deg out-of-phase on the opposite side of the plume but additional measurements are required to clarify the three-dimensional shear-layer structure.

C-mode plume interaction is strongest for the large nozzle spacing. Figure 10 shows a complete cycle for $s/d = 3.0$ and $M_j = 1.56$. The field of view is insufficient to see beyond the third shock cell, but the symmetric plume oscillation and intense density perturbation between the plumes are clearly shown. The wave fronts between the plumes are nearly planar, which is generally true for strong interaction between the jets. Figure 11 shows the same configuration at $M_j = 1.27$, where the helical motion of both plumes is of the same sense. In this special case the screech amplitude is reduced, but is greater than that of isolated jets.

Fig. 8 Schlieren visualization of coupled B mode; $s/d = 1.8$, $M_j = 1.31$, side view.

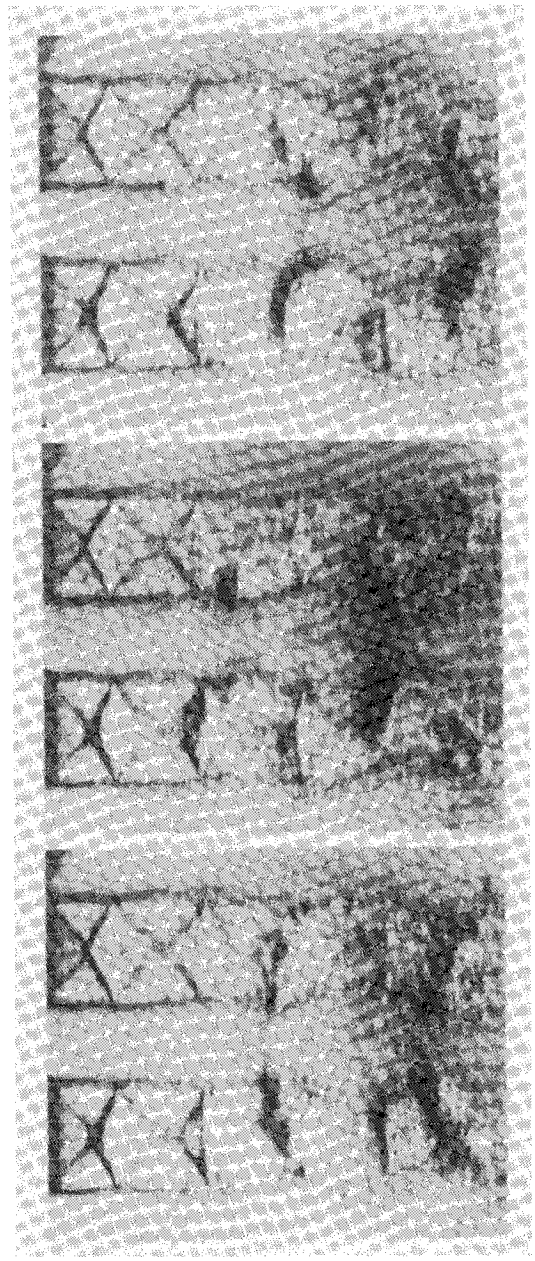

Fig. 9 Shadowgraph visualization of coupled B mode: $s/d = 1.7$, $M_j = 1.31$, unspecified increasing phase.

Velocity Measurements

Phase-conditioned, two-component LDV measurements were obtained in the plane of the jet centerlines for the peak interaction condition $s/d = 1.8$ and $M_j = 1.31$. Figure 12 is a shaded contour representation of the axial velocity in the jet core flow, with the darkest gray level representing a velocity of 425 m/s and white representing velocities below 325 m/s. The upper edge of the jet is the side between the plumes where the greatest shear-layer activity was observed in the flow visualization.

The velocity data support the observation that high-amplitude oscillation of the plume core occurs downstream of the second shock cell. In this case, the shocks are made visible by the low-velocity white regions that follow them. The shock motion observed in the flow visualization is expressed as lateral undulation of the core. Core displacement increases relative to the local core diameter with increasing distance from the nozzle. Increasing core displacement is a consequence of turning through multiple shocks and interaction with the growing shear-layer disturbances. The undulations of the core edge propagate downstream and are 180 deg out-of-phase across the jet core. The inner shear-layer edge is more distorted than the outer edge, which is consistent with the strong

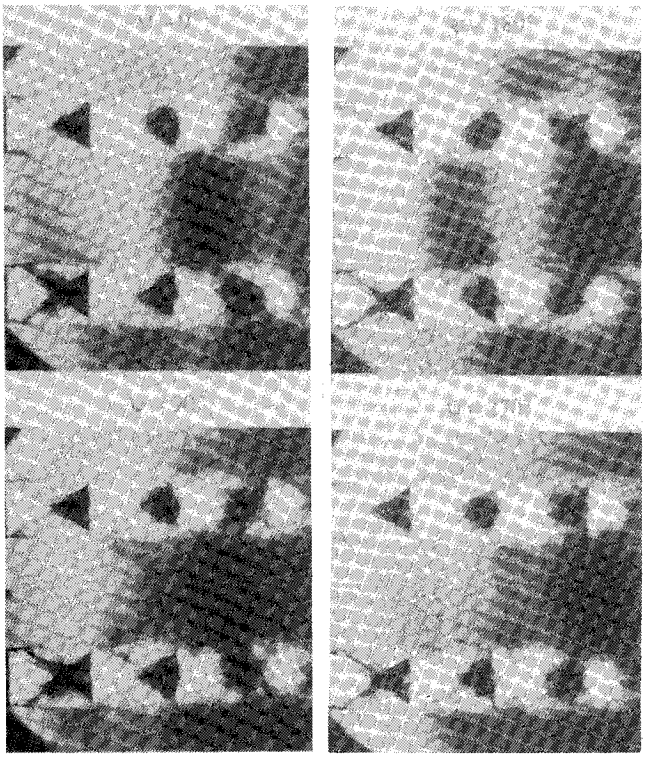

Fig. 10 Schlieren visualization of coupled C mode; $s/d=3.0$, $M_j=1.56$.

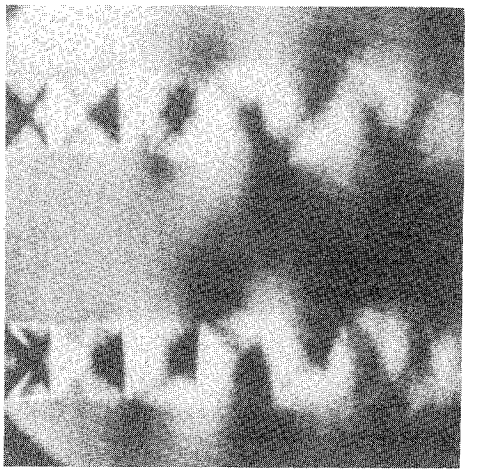

Fig. 11 Schlieren visualization of antiphase B-mode coupling; $s/d=3.0$, $M_j=1.27$.

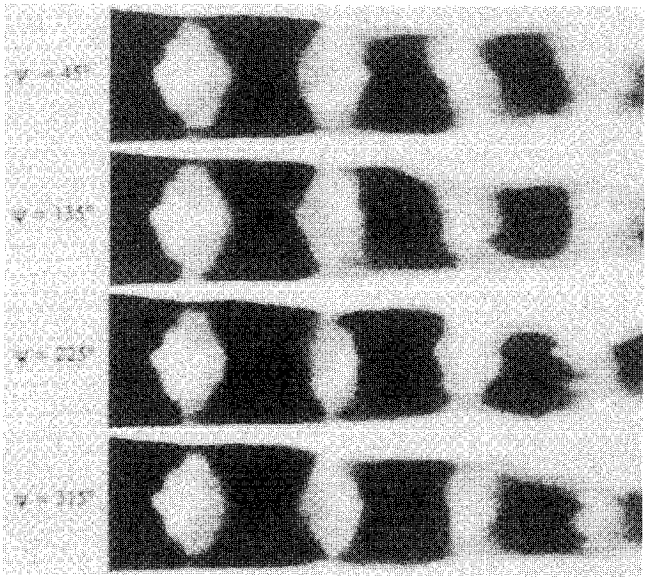

Fig. 12 Phase-conditioned axial velocity for coupled B mode; $s/d=1.8$, $M_j=1.31$, velocity range 325 m/s $\leq U \leq$ 425 m/s.

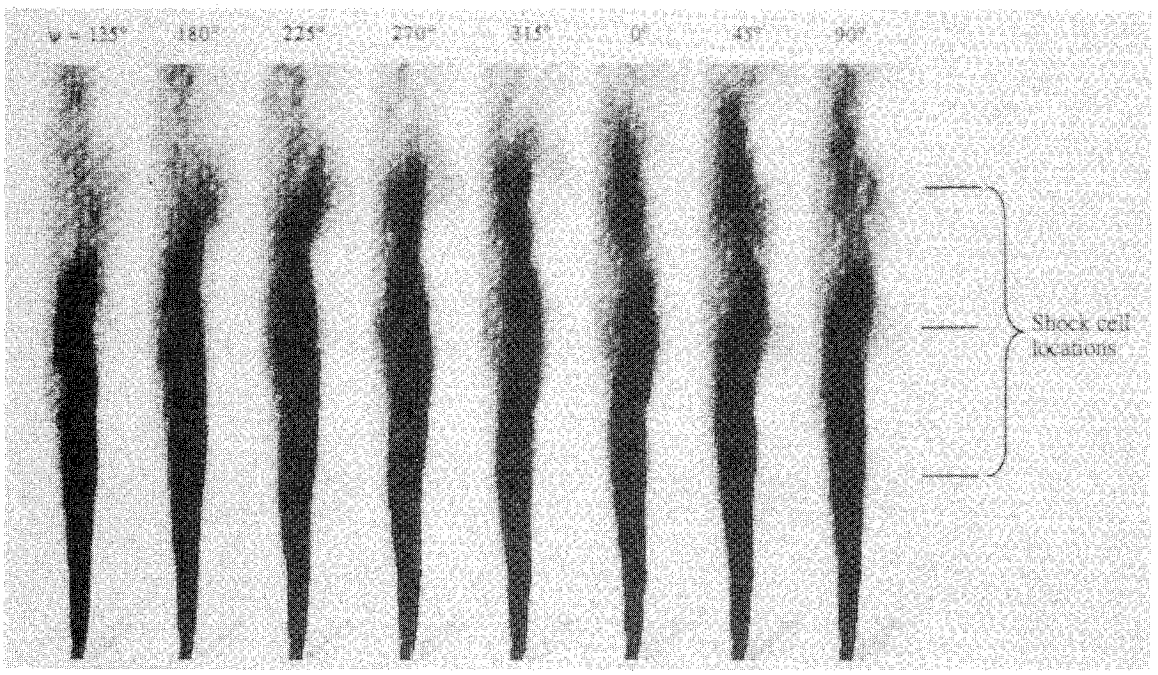

Fig. 13 Phase-conditioned vorticity distribution for coupled B mode; $s/d=1.8$, $M_j=1.31$; jet core is to right of layer, second plume is to left.

disturbance that appears between the jets in the shadowgraph pictures.

The phase-conditioned vorticity in the shear layer (Fig. 13) verifies that discrete concentrations of vorticity constitute the shear-layer disturbances that interact with the shocks in the screech process. Between the second and third cells, the shear layer is displaced over a range of approximately $d/3$ in the radial direction over one cycle. Beyond the third shock cell, the shear layer contains a concentration of vorticity that convects downstream at approximately half the core-flow velocity. A vorticity concentration appears in the exterior segment of the shear layer 180 deg antiphase to that in Fig. 13, as would be expected in a helical vortex.

Conclusions

The noise produced by mutual interaction of two supersonic plumes is a strong function of nozzle spacing and jet Mach number, with the design Mach number playing virtually no role in the process. Close spacing supports axisymmetric A1 and helical B modes, but suppresses the C mode relative to isolated plumes. Wide spacing inverts the modal dominance, and significant C-mode agumentation is observed.

When the plumes are in close proximity, each becomes a sound source for the feedback loop. The phase relationship between the sources must be such that they reinforce each other at the sites where the shear layer is receptive to acoustic disturbances. The phase-conditioned flow visualization shows that the acoustic wave fronts are nearly planar between the plumes when the resonant interaction is greatest.

Interference between the plumes is important in the selection of a dominant resonant mode. Visual evidence suggests that the A1 shear layer perturbations propagate from the nozzle lip; the B mode disturbances do not appear until after the first shock. There is a discontinuous increase in screech frequency from the B to the C mode, even though the shock-cell lengths are increasing. It is proposed that, for the B and C modes, the intersections between shocks and the shear layer are the sites at which the shear layer is receptive to acoustic feedback. These sites move farther downstream with increasing jet Mach number.

When nozzle spacing is small the plumes merge before the higher modes develop, and screech is thereby suppressed. When the spacing is large, the dominant modes develop farther downstream where the shear layers are thick. Thus a viable strategy for screech reduction may be to further reduce nozzle spacing to suppress B-mode interaction. The maximum afterburner configuration in Ref. 5 has an s/d ratio of 1.3; no plume coupling was observed over the entire range of M_j.

The phase-averaged velocity and vorticity measurements verify that vortical disturbances are responsible for screech. Vorticity concentrations similar to those observed in low-speed jets are excited in the shear layer and convect through the shock fronts. The vortex system for B mode is consistent with a helical jet instability. The jet core undergoes large amplitude oscillatory motion downstream of the second shock cell. This motion may be responsible for the high screech amplitudes at the nominally shock-free nozzle design pressure ratio.

The results presented here demonstrate that the plume coupling mechanism is complex, and that relatively small changes in nozzle geometry can have a large effect on the amplitude of the dynamic pressure. This high sensitivity to geometry suggests that effective measures can be devised to reduce plume interaction effects.

Acknowledgment

This work was performed under the McDonnell Douglas Independent Research and development program.

References

[1]Seiner, J. M., "Advances in High-Speed Jet Aeroacoustics," AIAA Paper 84-2275, 1984.

[2]Clauss, J. S., Wright, B. R., and Bowie, G. E., "Twin-Jet Noise Shielding for a Supersonic Transport," AIAA Paper 79-0670, 1979.

[3]Berndt, D. E., "Dynamic Pressure Fluctuations in the Internozzle Region of a Twin-Jet Nacelle," Society of Automotive Engineers, Narrendale, PA, TP-841540, 1984.

[4]Seiner, J. M., Manning, J. C., and Ponton, M. K., "Dynamic Pressure Loads Associated with Twin Supersonic Plume Resonance," AIAA Paper 86-1539, 1986.

[5]Seiner, J. M., Manning, J. C., and Ponton, M. K., "Model and Full-Scale Study of Twin Supersonic Plume Resonance," AIAA Paper 87-0244, 1987.

[6]Wlezien, R. W. and Kibens, V., "The Influence of Nozzle Asymmetry on Supersonic Jets," AIAA Paper 86-0277, 1986.

[7]Powell, A., "On the Mechanism of Choked Jet Noise," *Proceedings of the Physics Society B*, Vol. 66, 1953, pp. 1039-1056.

[8]Davies, M. G. and Oldfield, D. E. S., "Tones from a Choked Axisymmetric Jet," *Acoustica*, Vol. 12, 1962, pp. 257-277.

[9]Norum, T. D., "Screech Suppression in Supersonic Jets," *AIAA Journal*, Vol. 21, 1983, pp. 235-240.

[10]Seiner, J. M., Manning, J. C., and Ponton, M. K., "The Preferred Spatial Mode of Instability for a Mach 2 Jet," AIAA Paper 86-1942, 1986.